Pseudophakic Eye Models

5

Filomena Ribeiro, Pedro Ceia, and Leonor Jud

Introduction

Vision has always been a subject of interest for humans. Since the times of ancient Greece, with Democritus and Galenus being the most notable ones, to the Arabic scholars and Renaissance Europe through the work of Descartes, or more recently Snell's law and Gauss' paraxial theories, studies were conducted and theories were formulated to explain such a phenomenon and its properties [1, 2]. From the description of the detailed eye anatomy to the explanation of the optical system, step by step and aided by many developed instruments, human knowledge of vision has increased to an extent where one can expect to fully understand its functioning.

Eye models are necessary to study the optical characteristics of the human eye and to assess its diagnostic and therapeutic implications. The evolution of lens surgery and the development of different optical principles in intraocular lenses demand methods to select the most suitable intraocular lens (IOL) and predict the optical quality outcomes.

Pseudophakic eye models, with a realistic assessment of anatomy and visual performance in real life, when compared to the assessment using an optical bench or through interferometry, have been developed with several applications in ophthalmic implants. Possible clinical applications include IOL power calculation for cataract surgery, aspherical IOL power calculation, and the future development of customized lenses for full correction of optical aberrations.

Generic models have been successfully used for a variety of applications and have been very helpful for both diagnostic and therapeutic developments. However, only the emergence of personalized models and their subsequent clinical applications will pave the way for future customization.

Schematic Eye Models

The first schematic eye model dates back to the nineteenth century, even though previous attempts had already been made [2, 3]. Since then, many others were formulated, each pretending to approach and solve particular questions.

F. Ribeiro (✉)
Hospital da Luz Lisboa, Lisbon, Portugal

Faculdade de Medicina da Universidade de Lisboa, Lisbon, Portugal

Visual Sciences Research Centre, Lisbon, Portugal

P. Ceia
Faculdade de Medicina da Universidade de Lisboa, Lisbon, Portugal
e-mail: pedro.ceia@campus.ul.pt

L. Jud
Instituto Superior Técnico, Universidade de Lisboa, Lisbon, Portugal

J. Aramberri et al. (eds.), *Intraocular Lens Calculations*, Essentials in Ophthalmology,
https://doi.org/10.1007/978-3-031-50666-6_5

In order to summarize and organize our ever-growing understanding of the eye as an optical system and to study particular properties of human optics and retinal image formation, various authors have dedicated their work to the development of schematic eye models [3]. Their purposes range from the study of retinal image sizing to light levels, refractive errors, aberrations and retinal image quality, design of spectacles, lenses, and individual customization, or even development and calibration of optical instruments [1]. In order to account for different populations, they can even be stratified by age, gender, ethnicity, refractive error, and accommodation and allow total customization [1]. As much as each model is different, the same applies to their intended purposes and focus.

As complex as theoretical eye models may be, they can essentially be grouped into two types: Paraxial models and finite models.

Paraxial Models

Paraxial models are simpler ones. They mechanistically summarize what we know about the optics of the eye [1] while describing refractive surfaces as spherical and centered on a common optical axis. Refractive indices are constant within each medium too [2]. Such models are only accurate within the paraxial region and are not capable of predicting aberrations and retinal image formation for large pupils or angles that are far from the optical axis. Since structures are centered and refractive surfaces are spherical while the lens is generally of a constant refractive index, paraxial models are poor predictors of monocular aberrations such as spherical aberrations and sagittal/tangential power errors and lack the ability to predict light distribution with larger field angles [2]. Nonetheless, they are sufficient for calculation of the entrance and exit pupil positions and diameters as well as retinal image sizes and effects of on-axis low-order aberrations. For this reason, they are commonly used as a learning tool for the theory of visual optics [1].

At last, paraxial models may be further divided into three groups as follows, according to the number of refractive surfaces that each offers [1, 3, 4].

Reduced Paraxial Models

Reduced eyes have a single refractive surface—the cornea–along with a shorter axial length and corneal radius of curvature. In these models, principal points (P and P′) and nodal points (N and N′) coincide since there is only one refractive surface. As a consequence of the absence of the crystalline lens, they cannot be used to examine the optical consequences of accommodation nor the changes in lens property changes in refractive errors, including aphakia [2]. Some examples are Emsley's and Bennett and Rabbetts' reduced eyes.

Simplified Paraxial Models

Simplified models have a total of three refractive surfaces—one for the cornea and two for the lens. For paraxial calculations, these models are now considered to be more adequate than many exact eyes, which are more complex than is required.

- Gullstrand's number 2 eye (1909): Although close to its exact counterpart, its lens (even though two-surfaced) has zero thickness, which limits its usefulness.
- Le Grand's simplified eye (1945): This is similar to Gullstrand's number 2 eye in terms of features.
- Gullstrand–Emsley eye (1952): This is modified from Gullstrand's number 2 eye to simplify calculations, including the same lens thickness as in Gullstrand's number 1 eye, while also changing the aqueous, vitreous, and lens refractive indices. This model offers two accommodation levels as does Gullstrand's number 2 eye, but the lens' refractive index is constant.
- Bennett and Rabbetts' simplified eye: This is a modification from the Gullstrand–Emsley eye in its relaxed form with different parameter values obtained through data from a larger study, with a mean power closer to 60 D. It also includes four levels of accommodation, an "elderly" version of the eye, and a refractive error of 1-D hypermetropia.

Exact Paraxial Models

Exact models represent the optical structure most accurately as possible, and, so, they must include at least four refractive surfaces: two for the cornea and two for the crystalline lens.

- Tscherning (1900): This is allegedly the first model to include a posterior corneal surface.
- Gullstrand's number 1 eye (1909): This is built with six refractive surfaces, of which the lens is composed of four, divided into a higher refractive power nucleus and a lower power cortex, accounting for refractive index variation within the medium. Therefore, it has a gradient index lens. It also offers adaptation to two levels of accommodation, being one of the few paraxial models that have this particularity. Despite that, Gullstrand's model presents an exaggerated spherical aberration, much higher than that of real eyes.
- Le Grand's full theoretical eye (1945): As a modification of Tscherning's, this is presented in both relaxed and accommodated forms.
- Blaker's eye (1980): Modified from Gullstrand's number 1 eye, this is the only paraxial model to feature a continuous gradient index for the lens. This is also called an adaptive model since parameters such as lens gradient index, lens surface curvature, thickness, and the anterior chamber depth (ACD) vary as linear functions of accommodation. This model was posteriorly revised to include aging effects.

Finite Eye Models

Finite models are more complex than paraxial models, and their primary interest is a reliable representation of the eye's functional capabilities instead of its constitution. They may be used for simulating human optics more accurately, and different models may be designed for different purposes. Their aim is to represent optical aberrations and retinal quality as closely as possible as they occur in vivo, incorporating aspheric surfaces [5–8], chromatic dispersion [5, 8], and a refractive index gradient lens [5], and may even include accommodation [5], age-dependent changes [9], or refractive error dependency [10, 11]. These models are called finite models, or wide-angle models, and have greatly contributed to improve the knowledge of the human eye's real optical performance and to the development of better technologies.

Applications of such models are various, including calculations of retinal image sizes, magnification, retinal illumination, entrance and exit pupil positions, and diameters for objects imaged with wide pupils or away from the optical axis. Finite eye models can also be used for a range of research and development purposes, including ophthalmic lens design, refractive surgery or IOL implantation, and studying the features of optical component systems [12].

- Lotmar (1971): This model was modified from Le Grand's full theoretical eye with anterior corneal aspherization and a paraboloid posterior crystalline surface, to provide clinical levels of spherical aberration. However, it was shown that an ellipsoid shape for the anterior corneal surface would be a better fit and that the model is based on an anatomically inaccurate shape for the anterior lens surface.
- Drasdo and Fowler (1974): Based on a schematic eye attributed by Stine to Cowan, the purpose of this model was to determine retinal projection from the visual field using spherical lens surfaces since data supported the insignificance of such alteration.
- Kooijman (1983): Based on Le Grand's full theoretical eye, this predicts retinal illumination and adds aspheres to all four surfaces of the model. Corneal surfaces are aspherical, and the anterior lens surface is hyperbolic, whereas the posterior surface is parabolic. This model has two versions with retinal shape variations: spherical and elliptical.
- Liou and Brennan (1997): This model includes conicoid corneal and lenticular surfaces and a parabolic gradient index lens and is based on the average anatomical values of 45-year-old eyes if the parameter used is age-dependent. Its primary purpose was to model the spherical aberration of real eyes while also intending

to mimic normal levels of chromatic aberration—which was not successful. Additionally, it features a displacement of the aperture stop 0.5 mm to the nasal side and an angle of 5° between the line of sight and the optical axis regarding real eyes.
- Navarro and Escudero-Sanz (1999): This is a variable-accommodating model in which the lens parameters and anterior chamber depth are expressed as functions of accommodation in a logarithmic manner, based on Le Grand's full theoretical eye slightly modified for different anterior corneal radii and corneal indexes. Anterior corneal and lenticular surfaces are conicoids, whereas the retina is spherical.
- Atchison (2006): Based on Liou and Brennan's, a model was proposed to account for the displacement of the retina from the visual axis. The most distinctive features are the inclusion of a toric retina and its variation with refractive errors [4, 12].

Comparison of Finite Model Eyes

The abilities of different finite model eyes to evaluate the quality of vision have been discussed. Liou–Brennan and Atchison's models show the most similarities to in vivo eyes [12]. Lotmar's, Kooijman's, and Navarro and Escudero-Sanz' attempts were as accurate as Liou–Brennan's and Atchinson's at mimicking the real eye's performance reasonably well for on-axis and small-pupil diameters. For large-pupil diameters, however, the first ones were very inaccurate. Opposingly, Liou and Brennan and Atchison created schematic eyes that presented close-to-experimental in vivo values among spherical and higher order aberrations, even eccentrically, and peripheral refraction profiles for larger pupil diameters. Their corneal and lens spherical aberration and coma were similar but opposite in sign, which results in a good real eye representation [13]. Of the two models, Liou–Brennan's was considered the most reliable both anatomically and practically, even without considering the characteristic pupil nasal decentration [12, 14]. If lens and retina tilt and retinal decentration are taken into account, then Atchison's model has a peripheral refraction profile that does not match real eye data well. Eccentric variation of coma-like aberration was much higher than expected in every model as well as retinal image quality probably due to the lack of scattering among the optical media [12].

Computational Eye Models

Computational eye models hold the promise of becoming a primary tool to optimize the selection of the IOL to be implanted in a cataract procedure, for they are excellent predictive tools for the optical quality in pseudophakic eyes, allowing for a better understanding of contributory factors.

Physics and mathematical models require an optical design software such as Zemax (Zemax Development Corporation, Bellevue, WA), Code V (Optical Research Associates, Pasadena, CA), OSLO (Lambda Research Corporation, Littleton, MA), or ASAP (Breault Research Organization, Inc., Tucson, AZ), for both the construction of models and optical analysis and optimization based on ray tracing technology.

The increasing performance of computers has consequently boosted the area of computer simulation. Ray tracing is a very promising technology which, along with wavefront technology, better describes the optics of the human eye and allows for exact calculations.

Previously, in order to use Gullstrand and Emsley models, it was necessary to reduce the number of surfaces represented for simplicity and ray tracing speed. However, nowadays computers can quickly ray trace eye models and more complexity can be added.

Even though paraxial ray tracing has been used in several studies, real ray tracing use has increased recently. This is due to increasing computational capacity and awareness of the importance of higher order aberrations and their current ability to be clinically measured.

It has also been used to go further in the study of optical phenomena and to allow the evaluation of the entrance pupil and optical properties of the eye [15], night vision [16], and extremely aberrated eyes as in keratoconus eye modeling [16].

Lens Data Editor

Edit Solves Options Help

	Surf:Type	Comment	Radius	Thickness	Glass	Semi-Diameter		Conic
OBJ*	Standard	OBJECT	Infinity	1.000000E+009		8.748867E+007		0.000000
1	Standard	INPUT BEAM	Infinity	50.000000		1.977588	U	0.000000
2*	Standard	CORNEA	7.770000	0.500000	CORNEA_L&B	5.000000	U	-0.180000
3*	Standard	AQUEOUS	6.400000	3.160000	AQUOSO/VITREO_L&B	5.000000	U	-0.600000
STO#	Standard	PUPIL	Infinity	0.000000	AQUOSO/VITREO_L&B	1.250000	U	0.000000
5*	Gradient 3	LENS-FRONT	12.400000	1.590000		5.000000	U	-0.940000
6*	Gradient 3	LENS-BACK	Infinity	2.430000		5.000000	U	0.000000
7*	Standard	VITREOUS	-8.100000	16.270000	AQUOSO/VITREO_L&B	5.000000	U	0.960000
IMA	Standard	RETINA	-12.000000	-		5.000000	U	0.000000

Fig. 5.1 Zemax lens data editor with data from the Liou–Brennan model. The rows describe the object (OBJ), the surfaces of cornea (surfaces 2 and 3), pupil (STO; aperture stop), crystalline lens (surfaces 5 and 6), and the surface of retina (IMA). All surfaces are characterized by the radius of curvature (anterior and posterior), thickness, refractive index, chromatic dispersion, and asphericity. With this setup, light rays can be traced from the OBJ sequentially through the system to the IMA

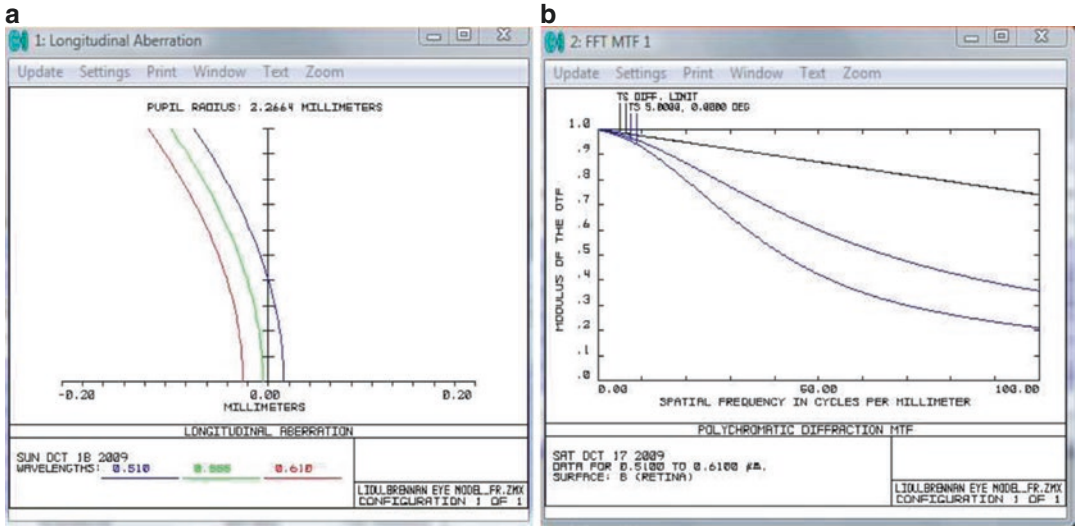

Fig. 5.2 Examples of optical performance evaluation using eye models. (**a**) Longitudinal chromatic aberration as a function of pupil height at each wavelength. (**b**) Polychromatic diffraction MTF (spatial frequency can be related to visual acuity measured by the Snellen chart, (considering that this chart has dark and bright bands subentending 1 minarc between them). For a visual acuity of 1.0, and considering a 100% contrast target, its correspondence to 100 cycles/mm may be established

Our research team published results [17] that identified the relative contribution of different optical elements to refractive error, using Zemax to model and evaluate the Liou–Brennan model (Figs. 5.1 and 5.2).

We used the Liou–Brennan eye model as a starting point, and its parameters were varied individually within a physiological range. The contribution of each parameter to the refractive error was assessed using linear regression curve fits. Formulas were obtained for each clinically measurable parameter, which represent the dioptric variation that each unit change on the optical element will cause (Table 5.1).

Table 5.1 Formulas for an easy and quick assessment of the effect of changes in each optical parameter on the refractive status of an eye, obtained by incorporating all of the aberrations of the eye. It should be noted that for the elements that did not show a good linear fit (corneal anterior radius, corneal posterior radius, and vitreous chamber depth), a variation around the nominal value or far from it will lead to different refractive errors. For instance, a small measurement error of corneal anterior radius below the nominal value may have more relevant repercussions on the refractive outcome than the same error above the nominal value

Optical element	Linear	Quadratic or inverse
Corneal elements		
Anterior radius (Ra)		$\mathbf{\Delta R_e}(D) = [-2.588(Ra) + 26.720]\ (\Delta Ra)$ (mm)
Posterior radius (Rp)		$\mathbf{\Delta R_e}(D) = [-37.384/Rp^2]\ (\Delta Rp)$ (mm)
Anterior asphericity (Qa)	$\Delta Re\ (D) = -1.120\Delta Qa$	
Posterior asphericity (Qp)	$\Delta Re\ (D) = 0.309\Delta Qp$	
Thickness (CT)	$\Delta Re\ (D) = -2.009\Delta CT$ (mm)	
Axial length elements		
Anterior chamber depth (ACD)	$\mathbf{\Delta R_e}\ (D) = -1.394\Delta ACD$ (mm)	
Lens thickness (LT)	$\mathbf{\Delta R_e}\ (D) = -2.414\Delta LT$ (mm)	
Vitreous chamber depth (VCD)		$\mathbf{\Delta R_e}(D) = [0.100(VCD) - 4.312]\ (\Delta VCD)$ (mm)
Pseudophakie eye		
Postoperative ACD (ACD_{post})	$\mathbf{\Delta R_e}\ (D) = -1.334\Delta ACD_{post}$ (mm)	

R_e refractive error; *D* diopter

Criteria for best-fit were r^2, *F* values, adjusted χ^2, and clinical significance. When values were similar, or when the difference between the linear fit and a more complex one was <10.251 diopters within a physiological range of the parameter variation, the linear fit was chosen. When all values were better for one of the models, that model was chosen. According to selection criteria, best fit was: linear for Qa, Qp, CT, ACD, and LT; quadratic for Ra and VCD; and inverse for Rp. A Δ preceding a parameter represents the variation of that parameter

Pseudophakic Eye Models

The growing developments in IOLs with new optical designs and corrective capabilities have not been on par with the methods that allow us to predict optical results. The previously mentioned models can be used for the evaluation of the pseudophakic eye, in which the lens is replaced by an IOL. In this new model, the complexity of the gradient refractive index of the crystalline lens is replaced by the IOL refractive index, the shape of the surfaces and optical design is made available by the manufacturer. All optical components of a pseudophakic eye are modeled by means of scientific computer methods so that physics and mathematical models can simulate and predict pseudophakic eye models' optics. With this methodology, the geometric optical properties, such as the wavefront aberration, can be simulated using Snell's refraction with ray tracing. The optical design process involves defining a conceptual optical design and giving an initial configuration input of the optical elements of the eye. The optical design software can be used to optimize an IOL by an iterative user-defined process to improve performance.

Real ray tracing has been used in several fields of ophthalmology to evaluate IOL performance on spherical aberration correction [18–22], interaction between monochromatic and chromatic aberrations [23], and aspheric intraocular lenses' optical performance in relation to tilt and decenter errors [24].

Personalized Pseudophakic Eye Models

The construction of personalized model and its subsequent clinical application will pave the way for future customization. The goal of eye modeling is to include the optical properties of one's entire eye into a complete custom virtual eye model. The modeling procedure of individual eyes is a complex task since it requires accurate biometric eye data such as the shape and thickness of the ocular elements.

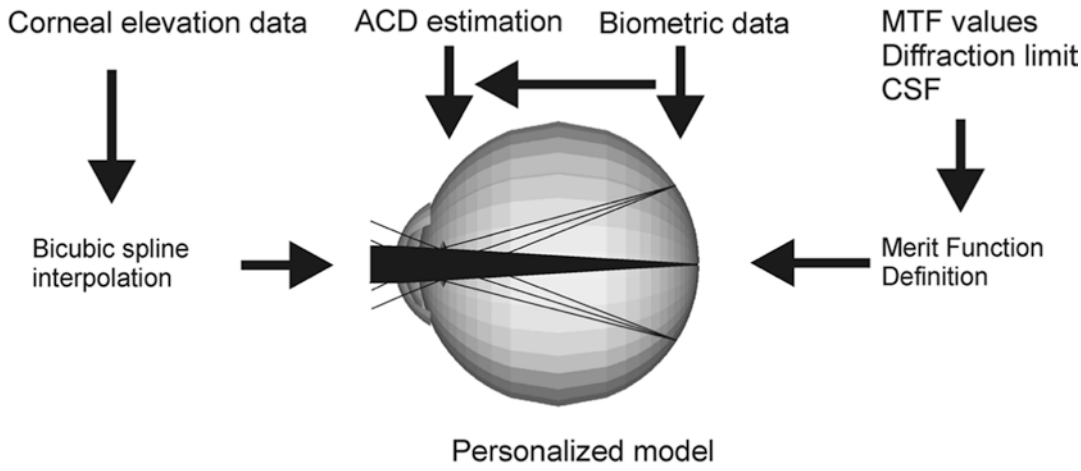

Fig. 5.3 An overview of the developed personalized pseudophakic model. The Liou–Brennan eye model was used as a starting point, and biometric values were replaced by individual measurements. Detailed corneal surface data were obtained from topography, and a grid of elevation values was used to define corneal surfaces in an optical ray tracing software (Zemax). Optimization criteria based on values of the modulation transfer function (MTF), weighted according to contrast sensitivity function (CSF), were applied

With the development of biometric measuring devices, we can accurately characterize the anterior and posterior surfaces of the cornea, intraocular distances, and aberrations of the ocular wavefront. All of these measurements can be incorporated into the construction of a customized model for functional optic nerve assessment.

The real ray tracing method may allow the highest degree of customization. Based on the principle that no single measurement of an eye can provide all the data required to achieve utmost individualization of therapeutic solutions, information from several sources, for example, corneal topography, corneal thickness, anterior chamber depth, lens thickness, and axial length, is considered. Some of its limitations are the current unavailability of measurements such as the shape of the lens, the retinal radius, the refractive indices of the ocular media and their relative distribution, and the lack of definition of the best optimization procedure.

Personalized models that can readily incorporate all these parameters as soon as our knowledge of them improves, or when measurement techniques become more accurate or available, will allow an easy progression toward customized refractive assessment. At last only the numerous stochastic errors associated with subjective examination will remain, along with IOL mislabeling errors and the uncertainty of how the interaction between higher order aberrations and neuroadaptation may influence refractive outcome.

Our research team has described the construction of personalized eye models, as seen in Fig. 5.3, which are based on the clinical measurement of individual human eyes [25], where computer-based technical implementation of the optical components and methods for calculations and optimizations in Zemax were implemented (Figs. 5.4 and 5.5). Optical optimization is the iteration algorithm that takes a starting optical design layout and changes the parameters in steps in order to achieve the specified targets.

IOL Power Calculation

One possible application is the calculation of intraocular lens power, with the potential to overcome the limitations of generic and population-related methods. This procedure can also be applied in the case of aspherical lenses and new optical designs.

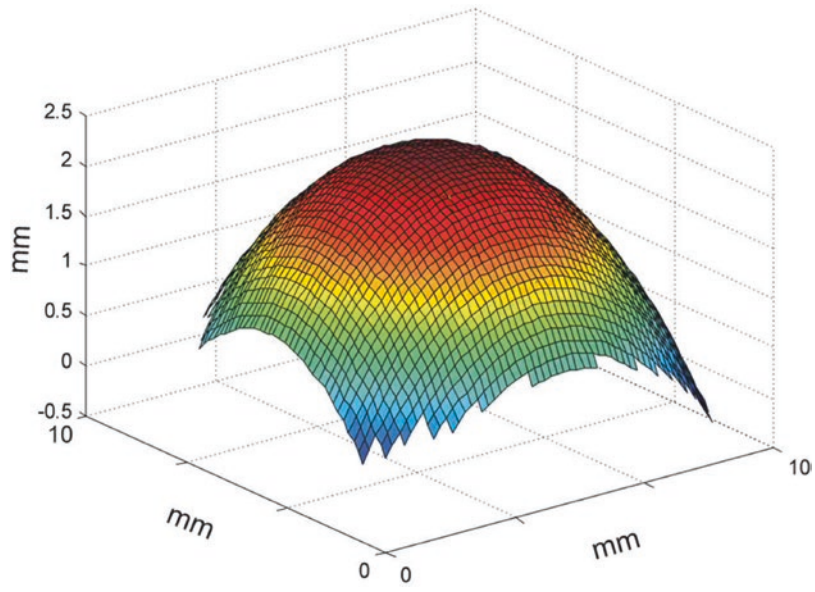

Fig. 5.4 Interpolated corneal elevation data for tridimensional corneal representation. Corneal elevation data generated from topography was re-formatted and imported to Zemax. Afterwards, a full definition of the surface shape was obtained through a bicubic spline interpolation of the imported data

Merit Function Editor: 9.000000E+009

Edit Tools Help

Oper #	Freq			Target	Weight	Value	% Contrib
1 MTFA	3.000000			0.990000	29.760000	0.000000	7.552573
2 MTFA	10.000000			0.950000	70.430000	0.000000	16.458738
3 MTFA	17.000000			0.920000	91.790000	0.000000	20.116974
4 MTFA	27.000000			0.870000	99.970000	0.000000	19.592950
5 MTFA	34.000000			0.840000	96.240000	0.000000	17.583520
6 MTFA	50.000000			0.770000	75.450000	0.000000	11.583301
7 MTFA	70.000000			0.680000	46.930000	0.000000	5.619013
8 MTFA	100.000000			0.550000	19.060000	0.000000	1.492932

Fig. 5.5 Merit function in which the used operands are the average MTF for different frequencies between 3 and 100 cycles/mm and the target is individually the system values by diffraction and the weights attributed depending on the CSF

Wavefront technology and ray tracing are very promising technologies that have been used to improve IOL power calculation errors [26–29], since they better describe the optics of the pseudophakic eye. Ray tracing allows for exact calculations, being simultaneously a better competitor when compared with paraxial optical methods, as long as the studied eye is properly modulated.

Since the calculation in the individual virtual eye is based on its complete geometry and is not limited to paraxial optics, it has the potential to overcome the limitations of current IOL calculation formulae and provide significant benefits to the eyes where current formulae are known to fail. This includes eyes that do not meet the population average such as eyes with irregular corneal surfaces as a result of refractive surgery (Fig. 5.6).

Possible clinical applications of this personalized model include the future development of customized lenses for full correction of optical aberrations (Fig. 5.7).

The results presented by our research group [25] suggest that the development of these eye models, considering individual aberrations, using wavefront technology and exact ray tracing, enhanced by the image metric based on MTF and CSF [30], allow for the prompt incorporation of parameters that are currently not measurable in clinical practice. This can be done in a personalized manner, if and when more clinical measurements become available, and can be incorporated,

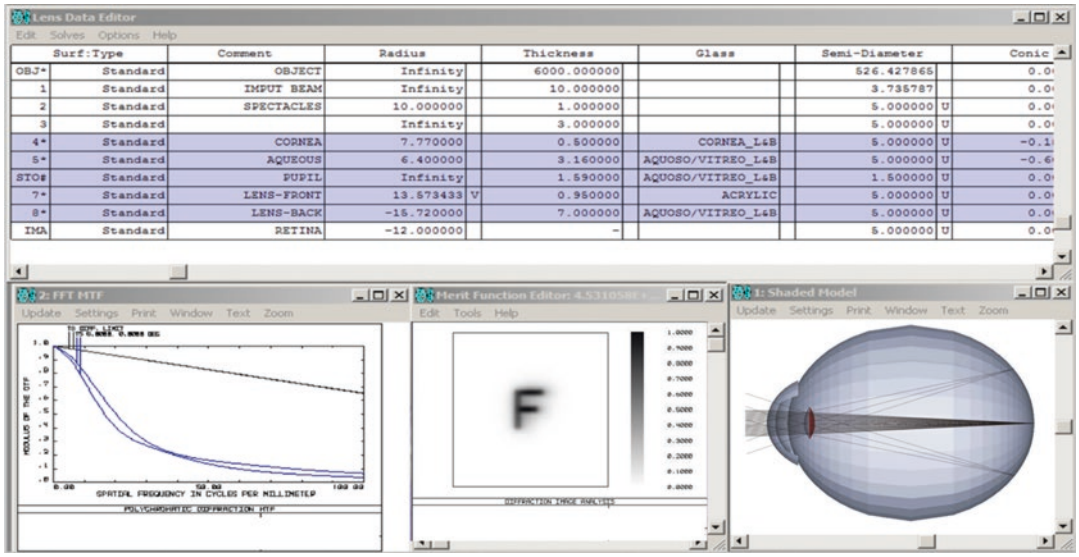

Fig. 5.6 Conversion in a pseudophakic model and its customization. Our model is prepared to incorporate all parameters in a personalized manner, as data becomes available in the clinical practice

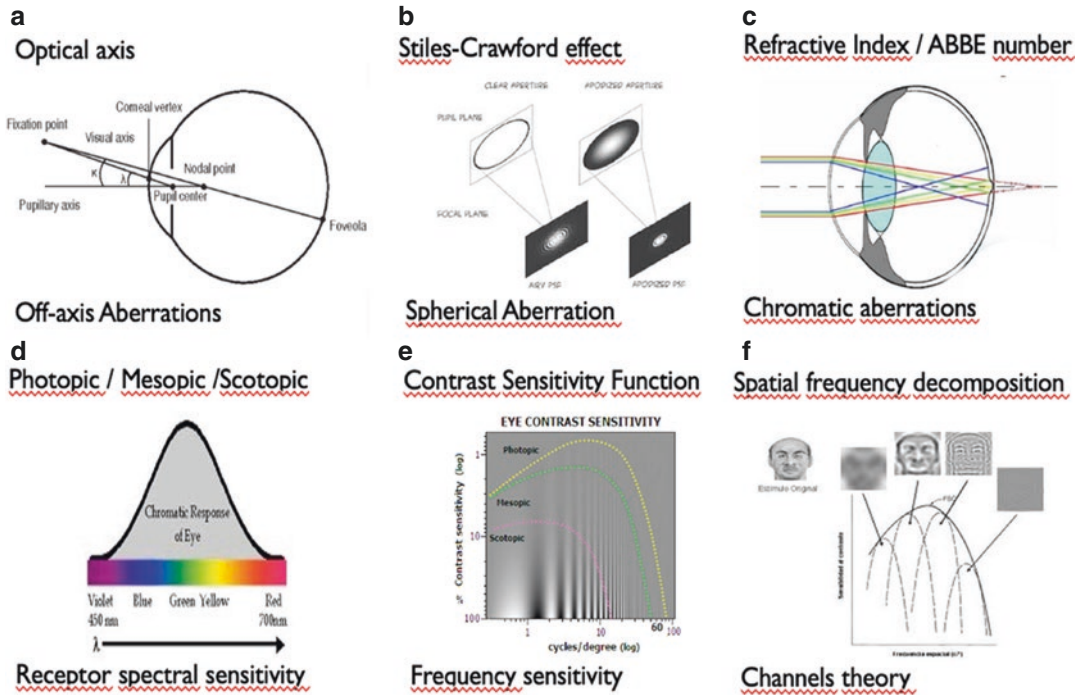

Fig. 5.7 Our optical phenomena simulation model for quality of vision evaluation. (**a**) Pupil decentration was set at 0.5 mm from the optical axis with a 5° angle between the visual and optical axis. (**b**) The Stiles–Crawford effect was incorporated as a Gaussian pupil apodization due to its relevance to eye aberrations. (**c**) In order to take chromatic dispersion into account, refractive indexes are calculated according to wavelength. (**d**) Receptor photopic spectral sensitivity was simulated using 510-, 555-, and 610-nm wavelengths, with relative weights of 1, 2, and 1, respectively. (**e**) The human CSF with a typical band-pass filter shape peaking at the spatial frequency at which the human eye is more sensitive in detecting contrast differences. The metric optimization defined different weights to each frequency (up to 100 cycles/mm, which corresponds to Snellen's 10/10 visual acuity) (**f**) in accordance with channel theory, which establishes that the visual pathway decomposes light in frequencies

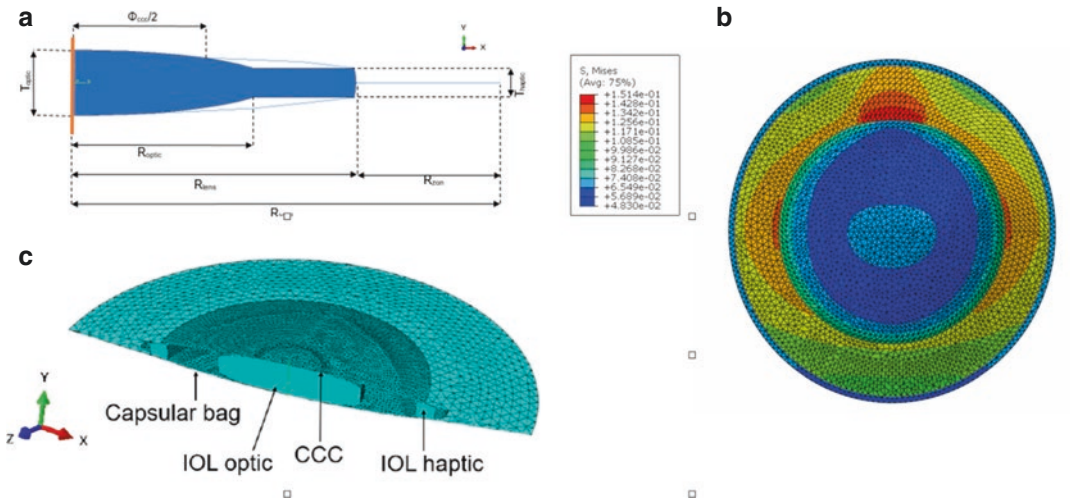

Fig. 5.8 Our models developed for the capsular bag–IOL complex: (**a**) axisymmetric geometry of the capsular bag–IOL complex [39]; (**b**) a finite element model of a three-dimensional pseudophakic [40]; and (**c**) von Mises stress (MPa) in the crystalline lens complex due to weakened zonular fibers

without the need for redefining population correction factors.

Pseudophakic Finite Element Models

The construction of biomechanical computational models of the human eye aims to understand its behavior in mechanical and optical terms. Finite element (FE) numerical simulation is an effective tool for analyzing phenomena that cannot be clarified by experimental methods, like most of the biomechanical processes.

This procedure has been applied in different anatomical features of the eye, such as the cornea [31] and the crystalline lens [32].

These simulations, however, depend heavily on the existence of experimental and clinical measurements, in order to provide the necessary data and validate the computational models' accuracy.

In order to portray the biomechanical behavior of the cornea, several in silico studies have been conducted. The condition of corneal ectasia and its response to cross-linking treatment [31] as well as the impact of laser ablative surgery on the long-term weakening of the corneal structure [33] and the implantation of intra-corneal ring segments have been assessed [34]. Other studies aimed to understand the biomechanics of the optical nerve head [35] and how it is influenced by scleral thickness [36].

Concerning the crystalline lens, initial studies compared the two main theories of accommodation: Helmoltz's and Schachar's [37]. Recent studies aim to understand the change of properties of the lens with age and their influence on presbyopia [38].

Computational models of the complete crystalline complex were already built but none for the pseudophakic eye. Our research group [39, 40] aimed to validate the previous knowledge of a healthy crystalline lens and to understand the biomechanical performance of the capsular bag and the effects of the implantation of an intraocular lens in cataract surgery (Fig. 5.8). With the objectives of modeling the new lens complex after surgery for removal of the cataractous lens, different configurations of IOL and capsular tension rings (CTR) can be considered as well as their position in the eye complex. This procedure can be applied to healthy and weakened zonular fibers in order to determine which mechanical factors contribute to capsular bag dislocation.

Furthermore, modeling of a pseudophakic eye can be relevant to understand behaviors that cannot be simulated experimentally, such as the

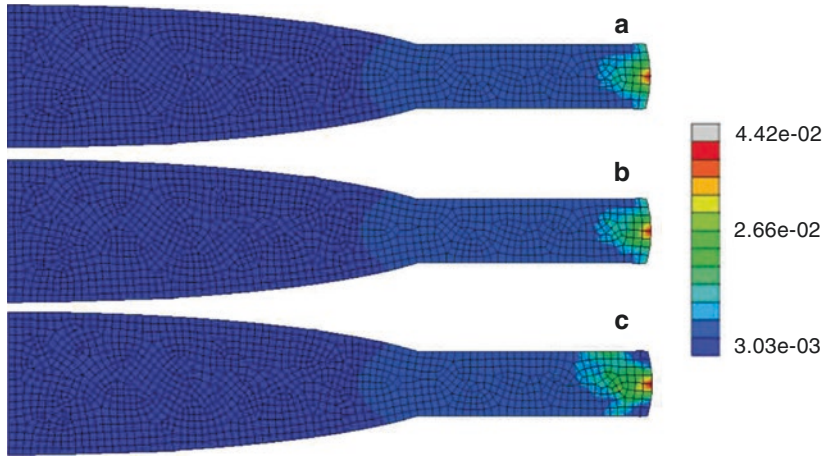

Fig. 5.9 von Mises stresses (in MPa) in the IOL for three different materials: (**a**) acrylic hydrophilic; (**b**) acrylic hydrophobic; (**c**) PMMA, after cataract surgery. All simulations were modeled with a 4-mm circular continuous capsulorrhexis [39]

assessment of the force acting on the IOL–capsular bag complex (Fig. 5.9).

The use of finite element analysis allows the search for solutions with great complexity that can support the experimental knowledge obtained so far. The underlying know-how for in silico experimentation is the subdivision of the modeled system into a number of small elements. For each of these elements, several equations are defined and solved, in order to understand the behavior of the structures both locally and globally, in terms of their geometric and mechanical alterations throughout the simulation.

However, these simulations require essential experimental knowledge in order to be accurately defined. Material properties of each of the system's components, geometric data, and boundary conditions are of utmost importance when defining the system's input data. Nonetheless, due to the computational effort that a simulation can require and lack of experimental data, some simplifications can be sometimes applied to the developed system.

Physical Eye Models

Wet-cell models with artificial cornea and IOL offer an alternative to schematic models, and they are often used in in vitro experiments. Although they perform well in evaluating ISO standards [41], they must keep up with the complexity of developing IOL designs and optics. New efforts are being developed to create physical models that better reproduce the anatomical and optical properties of a human eye.

Optomechanical eye models have been proposed to allow simulated in vivo testing of IOLs [42–44]. Also, due to the precision of three-dimensional printers and their flexibility at low cost, 3D physical models have been enhanced with the development in three-dimensional printing, with sliced images obtained with computed tomography [45] or defined with a 3D computer-aided design (CAD) [46]. Together with the main printed structure, poly(methyl methacrylate) (PMMA) aspherical corneas, variable iris, and IOLs can be assembled to a physical eye model.

Our research group has created a physical model of a custom-built pseudophakic eye to assess the accuracy of two commercially available measuring procedures of the pseudophakic anterior chamber (ACDpost) (Fig. 5.10). Knowing that OCT-based devices perform accurate measurements of anterior chamber depth (ACD), this technique will certainly contribute to improve intraocular lens position estimation methodologies and continue to push forward ray tracing-based methodologies, which make a direct use of the physical position of the IOL and

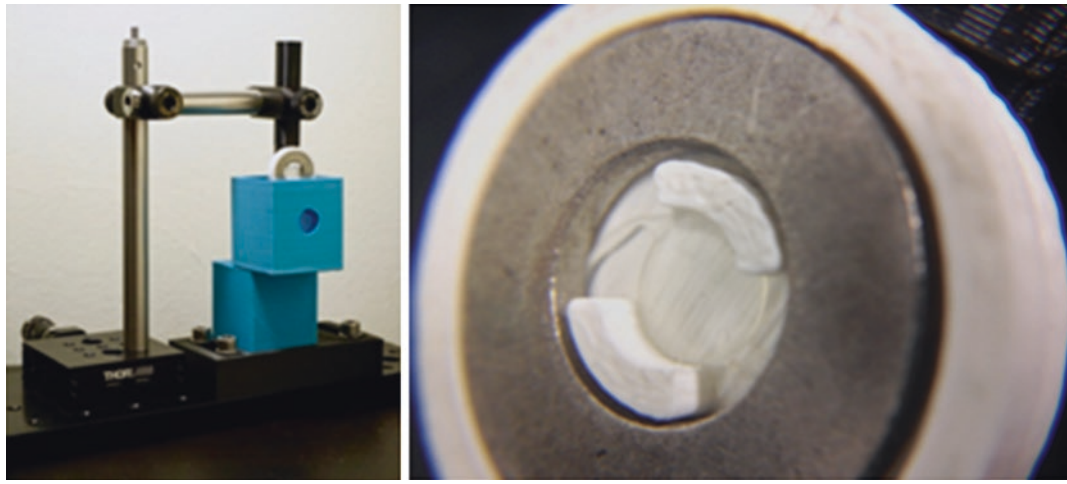

Fig. 5.10 A pseudophakic eye phantom and a custom IOL holder for micrometric axial displacements.

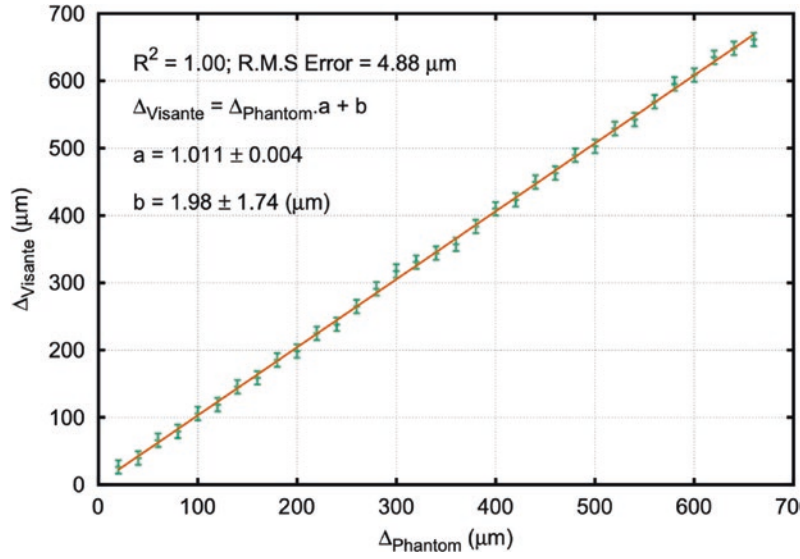

Fig. 5.11 Relation between Visante™ OCT and IOL's Phantom Eye relative displacement measurements in water with very good correlation

not the effective lens position (ELP). The phantom was built using laboratory-grade optomechanical components, custom-designed components, and a 22D SA60AT Alcon AcrySof single-piece IOL. The IOL was installed in a custom IOL holder, allowing for precise axial displacements relative to the front surface. Calibrations were performed, and the span shift error was found to be virtually nonexistent.

With this physical model we concluded that measurements obtained with the Haag-Streit Lenstar are interchangeable with those of the Zeiss Visante. Moreover, this device had issues regarding accurate measurement of the IOL thickness in vivo, which is probably due to the difficulty in detecting the reflection from its posterior surface combined with an eventual mismatch of the refractive index of the IOL (Fig. 5.11). It is important to be aware that an inaccurate IOL thickness measurement will propagate its error to posterior eye structures which impacts the accuracy of axial length measurements. As such, performing biometry with this device in pseudophakic eyes will likely result in

incorrect axial length measurements. Using the eye phantom, the performance of Visante device was also found to be superior with higher precision.

Conclusions

The modeling of anatomy, biomechanical properties, and optical phenomena are essential tools for the development of knowledge about the physiology of the pseudophakic eye and allow the development and validation of new therapeutic solutions for the final goal of customization for individual treatment.

References

1. Atchison DA, Thibos LN. Optical models of the human eye. Clin Exp Optom. 2016;99:99–106.
2. Smith G. Invited review schematic eyes: history, description and applications. Clin Exp Optom. 1995;78:176–89.
3. Atchison DA, Smith G. Optics of the human eye. 1st ed. Edinburgh: Butterworth-Heinemann; 2000.
4. Esteve-Taboada JJ, Montés-Micó R, Ferrer-Blasco T. Schematic eye models to mimic the behavior of the accommodating human eye. J Cataract Refract Surg. 2018;44:627–41.
5. Liou H-L, Brennan NA. Anatomically accurate, finite model eye for optical modeling. J Opt Soc Am A. 1997;14:1684.
6. Escudero-Sanz I, Navarro R. Off-axis aberrations of a wide-angle schematic eye model. J Opt Soc Am A. 1999;16:1881.
7. Kooijman AC. Light distribution on the retina of a wide-angle theoretical eye. J Opt Soc Am. 1983;73:1544–50.
8. Navarro R, Santamaría J, Bescós J. Accommodation-dependent model of the human eye with aspherics. J Opt Soc Am A. 1985;2:1273.
9. Norrby S. The Dubbelman eye model analysed by ray tracing through aspheric surfaces. Ophthalmic Physiol Opt. 2005;25:153–61.
10. Atchison DA. Optical models for human myopic eyes. Vis Res. 2006;46:2236–50.
11. Llorente L, Barbero S, Cano D, et al. Myopic versus hyperopic eyes: axial length, corneal shape and optical aberrations. J Vis. 2004;4:5.
12. Bakaraju RC, Ehrmann K, Papas E, et al. Finite schematic eye models and their accuracy to in-vivo data. Vis Res. 2008;48:1681–94.
13. Smith G, Bedggood P, Ashman R, et al. Exploring ocular aberrations with a schematic human eye model. Optom Vis Sci. 2008;85:330–40.
14. De Almeida MS, Carvalho LA. Different schematic eyes and their accuracy to the in vivo eye: a quantitative comparison study. Brazilian J Phys. 2007;37:378–87.
15. Aguirre GK. A model of the entrance pupil of the human eye. Sci Rep. 2019;9:9360.
16. Chen Y-L, Tan B, Baker K, et al. Simulation of keratoconus observation in photorefraction. Opt Express. 2006;14:11477.
17. Ribeiro F, Castanheira-Dinis A, Dias JM. Refractive error assessment: influence of different optical elements and current limits of biometric techniques. J Refract Surg. 2013;29:206–12.
18. Smith G, Pierscionek BK, Atchison DA. The optical modelling of the human lens. Ophthalmic Physiol Opt J Br Coll Ophthalmic Opt. 1991;11:359–69.
19. Werner W, Roth EH. [Image properties of spherical as aspheric intraocular lenses]. Klin Monatsbl Augenheilkd. 1999;214:246–50.
20. Altmann GE, Nichamin LD, Lane SS, et al. Optical performance of 3 intraocular lens designs in the presence of decentration. J Cataract Refract Surg. 2005;31:574–85.
21. Marcos S, Barbero S, Jiménez-Alfaro I. Optical quality and depth-of-field of eyes implanted with spherical and aspheric intraocular lenses. J Refract Surg. 2005;21:223–35.
22. Tabernero J, Piers P, Benito A, et al. Predicting the optical performance of eyes implanted with IOLs to correct spherical aberration. Investig Ophthalmol Vis Sci. 2006;47:4651–8.
23. Marcos S, Romero M, Benedí-García C, et al. Interaction of monochromatic and chromatic aberrations in pseudophakic patients. J Refract Surg. 2020;36:230–8.
24. Pérez-Gracia J, Varea A, Ares J, et al. Evaluation of the optical performance for aspheric intraocular lenses in relation with tilt and decenter errors. PLoS One. 2020;15:1–14.
25. Ribeiro FJ, Castanheira-Dinis A, Dias JM. Personalized pseudophakic model for refractive assessment. PLoS One. 2012;7:1–8.
26. Sun M, Pérez-Merino P, Martinez-Enriquez E, et al. Full 3-D OCT-based pseudophakic custom computer eye model. Biomed Opt Express. 2016;7:1074–88.
27. Olsen T, Hoffmann P. C constant: new concept for ray tracing–assisted intraocular lens power calculation. J Cataract Refract Surg. 2014;40:764–73.
28. Saiki M, Negishi K, Kato N, et al. Ray tracing software for intraocular lens power calculation after corneal excimer laser surgery. Jpn J Ophthalmol. 2014;58:276–81.
29. Rosales P, Marcos S. Customized computer models of eyes with intraocular lenses. Opt Express. 2007;15:2204–18.
30. Ribeiro F, Castanheira-Dinis A, Sanches JM, et al. Assessment of image quality using a pseudophakic eye model for refractive evaluation. Lecture Notes in Computer Science (Including Subseries Lecture Notes in Artificial Intelligence and Lecture Notes in Bioinformatics), vol. 7887. LNCS; 2013. p. 543–50.

31. Sinha Roy A, Rocha KM, Randleman JB, et al. Inverse computational analysis of in vivo corneal elastic modulus change after collagen crosslinking for keratoconus. Exp Eye Res. 2013;113:92–104.
32. Lanchares E, Navarro R, Calvo B. Hyperelastic modelling of the crystalline lens: accommodation and presbyopia. J Optom. 2012;5:110–20.
33. Sinha Roy A, Dupps WJJ. Patient-specific modeling of corneal refractive surgery outcomes and inverse estimation of elastic property changes. J Biomech Eng. 2011;133:11002.
34. Kling S, Marcos S. Finite-element modeling of intrastromal ring segment implantation into a hyperelastic cornea. Investig Opthalmology Vis Sci. 2013;54:881–9.
35. Sigal IA, Flanagan JG, Tertinegg I, et al. Finite element modeling of optic nerve head biomechanics. Investig Ophthalmol Vis Sci. 2004;45:4378–87.
36. Norman RE, Flanagan JG, Sigal IA, et al. Finite element modeling of the human sclera: influence on optic nerve head biomechanics and connections with glaucoma. Exp Eye Res. 2011;93:4–12.
37. Burd HJ, Judge SJ, Flavell MJ. Mechanics of accommodation of the human eye. Vis Res. 1999;39:1591–5.
38. Wang K, Venetsanos DT, Hoshino M, et al. A modeling approach for investigating opto-mechanical relationships in the human eye lens. IEEE Trans Biomed Eng. 2020;67:999–1006.
39. Cardoso MT, Feijó B, Castro APG et al. Axisymmetric finite element modelling of the crystalline under cataract surgery. 2019.
40. Paulino JS, Feijó B, Ribeiro FJ et al. 3D finite element modelling of the pseudophakic eye. 2020.
41. Alba-Bueno F, Vega F, Millán MS. Design of a test bench for intraocular lens optical characterization. J Phys Conf Ser. 2011;274:12105.
42. Gobbi PG, Fasce F, Bozza S, et al. Optomechanical eye model with imaging capabilities for objective evaluation of intraocular lenses. J Cataract Refract Surg. 2006;32:643–51.
43. Inoue M, Noda T, Mihashi T, et al. Quality of image of grating target placed in model of human eye with corneal aberrations as observed through multifocal intraocular lenses. Am J Ophthalmol. 2011;151:644–652.e1.
44. Inoue M, Noda T, Ohnuma K, et al. Quality of image of grating target placed in model eye and observed through Toric intraocular lenses. Am J Ophthalmol. 2013;155:243–252.e1.
45. Dobler B, Bendl R. Precise modelling of the eye for proton therapy of intra-ocular tumours. Phys Med Biol. 2002;47:593–613.
46. Xie P, Hu Z, Zhang X, et al. Application of 3-dimensional printing technology to construct an eye model for fundus viewing study. PLoS One. 2014;9:e109373.